Internal Annular Wall Jets: Radial Flow in a Stirred Tank

Suzanne M. Kresta and Kevin J. Bittorf
Dept. of Chemical and Materials Engineering, University of Alberta, Edmonton, Alberta, Canada, T6G 2G6

David J. Wilson
Dept. of Mechanical Engineering, University of Alberta, Edmonton, Alberta, Canada, T6G 26G

Similarity solutions are derived for internal annular wall jets and compared with experimentally determined velocity profiles at the wall of a stirred tank with radial flow. The first similarity solution considers a geometry where the thickness of the wall jet is small relative to the diameter of the cylinder and the fluid flows relative to a free stream velocity of zero. In the second solution, the free stream velocity opposes the direction of the jet flow, as is observed in the recirculating flow in a stirred tank. The internal annular wall jet model agrees very well with the flow at the wall of a stirred tank agitated with a Rushton turbine. The free stream counter flow is driven by the wall jet, and a single velocity and length scale define the self-similar velocity profiles for the flow in the jet and in the recirculating flow. Both the analytical model and experimentally observed expansion rates are linear and the maximum velocity in the jet decays as $[U \propto (z/T)^{-0.5}]$*, where* (z/T) *is the dimensionless streamwise distance. This decay can be contrasted with the faster decay* $[U \propto (z/T)^{-1}]$ *observed in the 3-D wall jets produced by axial impellers. These results provide a basis for validating computational fluid dynamic simulations in stirred tanks and for estimating the largest length scales of turbulence in the bulk of the tank.*

Introduction

The geometry examined in this work is a stirred tank agitated with a radial impeller. In this vessel, the impeller discharge stream impinges on the wall of the tank and divides into upward and downward circulations, each of which may form wall jets. In this article, we propose that the flow in the bulk of the tank can be modeled using a self-similar annular wall jet. Support for the annular jet hypothesis is drawn from three conditions: axisymmetry of the flow at the wall, self-similar mean velocity profiles that scale with the maximum jet velocity U_m, and jet half-width b, and jetlike decay of those scales as $U_m \propto 1/z^{0.5}$ and $b \propto z$, where z is the distance along the jet. The axisymmetric annular wall jet driven by the radial Rushton turbine appears in sharp contrast to the four discrete three-dimensional (3-D) wall jets that form when the flow is driven by axial impellers. Bittorf and Kresta (2001) show that the 3-D jets behave as one-quarter of a round jet, concentrated at the upstream side of each baffle and decaying with $U_m \propto 1/z$ and $b \propto z$. Description of the flow in the bulk of the tank in terms of wall jets allows reduction of a whole set of velocity profiles to a few key characteristics of the jet which apply over a large region of the tank.

The annular jet hypothesis has significant implications for understanding turbulence scaling in the bulk of the tank, solids distribution throughout the vessel, and changes in the flow field due to changes in impeller geometry, size, and off-bottom clearance. It also provides a framework for validation of computational fluid dynamic (CFD) modeling approaches, shifting the emphasis from accuracy of a single profile to correct scaling of velocity and length scales throughout a large region of the flow.

Prandtl's boundary layer (a driven flow near a solid surface) is the preeminent example of a distinctive region occurring as part of many complex flows. Like jets, the boundary layer can be understood in terms of a single characteristic length scale and a single characteristic velocity scale. While

Correspondence concerning this article should be addressed to S. M. Kresta.

boundary layers are a class of *driven* flows, jets represent a class of *driver* flows. Jets have been extensively examined in the literature, and wall jet theory dates back to Glauert's similarity solution, which was presented in 1956. Key characteristics of wall jets include similarity of velocity profiles, power-law decay of maximum velocity, and linear expansion of the jet with downstream distance due to entrainment of surrounding fluid. In this article, the similarity characteristics of the 2-D plane wall jet are extended to the case of an internal annular wall jet. This idealized flow is then used to further our understanding of the complex flow field in stirred tanks.

A 2-D plane jet can originate from either a line source (directed parallel to the flow) or a point source (at the center of a radial jet). The similarity solution for a wall jet originating from a line source was initially examined by Glauert (1956), who separated the similarity solution into two components: the inner (boundary) layer and the outer (jet) layer. Bakke's (1957) experiments on a 2-D plane wall jet confirmed Galuert's theoretical results. Since this time Chao and Sandborn (1966), Wilson and Goldstein (1976), and Launder and Rodi (1981, 1983) have examined the turbulence, the shear stress at the wall, and the decay and expansion of the plane wall jet. Launder and Rodi (1981, 1983) investigated the inner boundary-layer profile and found that it can be described by the logarithmic law of the wall. Recent studies by Abrahamsson et al. (1994), Eriksson et al. (1998), and Venas et al. (1999) have refined the results for the inner layer and the turbulent properties, and have provided additional confirmation of the decay and expansion behavior of the plane wall jet.

There have also been investigations of axial wall jets with cross-stream curvature that form on the outside of cylinders (Starr and Sparrow, 1967; Rajaratnam, 1976; Rodman et al., 1989) and the outside of other bodies of revolution (Sharma, 1981; Kolar et al., 1989). Rajaratnam (1976) and Starr and Sparrow (1967) derived expressions for the decay of a wall jet on the outside of a cylinder: an *external* annular wall jet. In the case of a large cylinder, the external jet decays like a plane jet. In the case of a small cylinder, the external jet decays like a round jet. The half-width, b, increases linearly with z, and the velocity decay depends on the radius of the cylinder, R, relative to the half-width of the jet, b. If $R \gg b$, then the decay of the maximum jet velocity (U_m) is inversely proportional to the *square root* of the distance traveled, $U_m \propto 1/z^{0.5}$. If $R < b$, then the decay of the jet velocity is proportional to the distance traveled, $U_m \propto 1/z$. Both of these results agree with an axial momentum balance where the wall shear stress is negligible.

Internal annular wall jets have not been studied before, perhaps because most cylindrical systems with internal flow are either small-diameter pipes, where annular jets rapidly grow into fully developed pipe flow; large diameter columns, where it is desirable to distribute the flow evenly over the full cross section; or wetted wall columns, where the annular flow ends at the gas–liquid interface. In stirred tanks, internal annular wall jets can form due to the combination of the large diameter of the vessel and the recirculating nature of the flow.

In this article, the equations of motion for the turbulent internal annular wall jet with zero free stream velocity, and with a counterflowing free stream or recirculation velocity *driven by the jet*, are developed and tested in the context of a stirred tank. The first section is devoted to developing the relevant equations for the internal annular jet and to deriving the jet decay and expansion coefficients. The second section extracts the velocity similarity profiles for the cases of zero free stream velocity and for the more realistic case of recirculating flow. The final section examines the experimental data for a stirred tank in the context of these theoretical developments.

Annular Jet Equations

Figure 1a shows an internal annular wall jet in a cylinder that is open at both ends. The jet is driven by flow through an annular slot of width S at the bottom of the section of interest. There is no recirculation, and the free stream velocity is zero. The thickness of the jet is initially much smaller than the radius of the cylinder. As the jet expands, it will eventually penetrate to the center of the cylinder. Downstream from this point, the internal annular wall jet will evolve into an axial flow with U_m migrating to the center of the pipe. The analysis which follows is restricted to the early part of the jet, where the jet width is much less than the radius of the cylinder and the center-line velocity is zero.

In a stirred tank, the recirculating flow plays an important role in the development of the wall jet. A second geometry, shown in Figure 1b, was used to develop equations for the case of recirculating flow with a *negative* free stream velocity. In this geometry, the top end of the cylinder is closed. The fluid enters through the annular slot at the bottom of the cylinder. The closed upper surface forces the fluid to recirculate and leave through the central opening at the bottom of

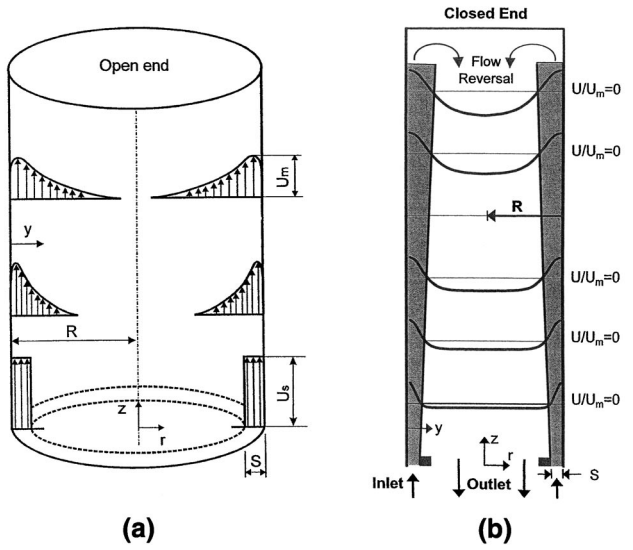

Figure 1. (a) Wall jet due to flow through annular slot inside a cylinder with stagnant fluid (cylinder radius, *R*, is larger than annular slot widths S, and both ends of the cylinder are open); (b) annular wall jet with recirculation (wall jet enters through an annular slot, as in (a), $R \gg S$, the top of the cylinder is closed and the bottom is open).

the cylinder. Since the flow is axisymmetric, the velocity gradient is always zero at the center of the tank, where the velocity is at its maximum negative value, U_R. Under steady flow conditions, the upward and downward volumetric flows along any traverse must be equal, since the flow entering the system is equal to the flow leaving the system. The flow in the jet expands and entrains fluid as it moves up the wall, and the jet flow must be balanced by the recirculating flow, which penetrates further and further toward the center of the tank as the wall jet expands. The similarity solution will fail once the jet has expanded to the point where the recirculating flow must accelerate to satisfy continuity. Beyond this point, U_R will not scale with U_m, and two characteristic velocity scales will be needed to characterize the flow. This is apparent in the top profile shown in Figure 1b. Further analysis of this case is provided by Bittorf (2000), but we restrict further consideration to the case where $b \ll R$, and U_R scales with U_m.

The equations for both internal annular wall jets are based on a 2-D formulation of the Reynolds Averaged Navier Stokes (RANS) equations. Derivation of the scaling of the velocity decay and jet expansion and of velocity profiles for the two boundary conditions of interest follows. The two critical boundary conditions for the jet are zero free stream velocity, as shown in Figure 1a, and recirculating flow with a negative free stream velocity, as shown in Figure 1b. The axes in Figures 1a and 1b show two sets of coordinates in the radial direction: y is the distance from the wall, and r originates at the axis of the cylinder. The reader will find that the wall-jet scaling is more conveniently expressed in terms of y.

Velocity decay and jet expansion

The derivation of the internal annular wall jet begins with the reduction of the RANS equations in cylindrical coordinates. The assumptions used in the reduction of the equations follow the usual boundary-layer approximations for turbulent jets:

- The flow is fully turbulent; hence, the viscous shear stress can be neglected relative to the turbulent stresses.
- Body forces are balanced by static pressure. When the model is applied to the stirred-tank geometry, this means that the suction pressure due to the action of the impeller will be neglected.
- The jet is axisymmetric ($\partial/\partial\theta = 0$), so tangential velocities within the jet are taken to be zero ($W = 0$).
- The boundary layer approximations require that the length scale in the radial direction is much smaller than the length scale in the axial direction, $\partial/\partial r \gg \partial/\partial z$, and the velocity in the axial direction is much larger than the velocity in the radial direction; $U \gg V$.

These assumptions are discussed in detail by Schwarz and Cosart (1960), Newman et al. (1972), Rajaratnam and Pani (1970, 1974), and Rajaratnam (1976), who give derivations similar to the annular jet derivation for other jet geometries.

Applying the boundary-layer approximation to the annular jet geometry, the radial (V) component of the RANS equations reduces to show that the radial dynamic pressure gradient is balanced by the Reynolds stress. The angular (W) component is zero, since there is no angular variation. The remaining equations are the axial (U) equation and the continuity equation:

$$U\frac{\partial U}{\partial z} + V\frac{\partial U}{\partial r} = -\frac{1}{r}\frac{\partial}{\partial r}\left(r\overline{uv}\right) \tag{1}$$

$$r\frac{\partial}{\partial z}U + \frac{\partial}{\partial r}(rV) = 0 \tag{2}$$

The next step is based on the assumption that the jet is self-preserving. Three similarity variables are used: The streamwise velocity (f'), the Reynolds stress (g) at a given cross-stream position, and the cross-stream distance (η). For the cross-stream position the r coordinate is not convenient: the distance from the cylindrical wall, ($y = R - r$) is used instead. Equation 3 gives the similarity variables:

$$\eta = \frac{y}{b} \qquad f'(\eta) = \frac{U}{U_m} \qquad g(\eta) = \frac{\overline{uv}}{U_m^2}. \tag{3}$$

Selection of the similarity variables U_m and b implies that the flow throughout the jet will be scaled by a single characteristic length scale, b, and a single characteristic velocity scale, U_m. The velocity scale U_m is the local maximum velocity at height z and b is the y location where $U = 0.5U_m$. The jet half-width b must be much less than R to avoid the development of pipe flow. Through substitution of Eq. 3 into Eq. 1, the equations of motion become:

$$g'\frac{U_m^2}{b} = \eta f f'\frac{U_m^2 b'}{b} - f^2 U_m U_m' + f' V\frac{U_m}{b} \tag{4}$$

Here $f' = df/d\eta$, $g' = dg/d\eta$, $b' = db/dz$, and $U_m' = dU_m/dz$. The continuity equation (Eq. 2) is used to solve for the radial velocity, V, and is substituted into Eq. 4, resulting in:

$$g' = b'\left(\eta f f' + f'\int \eta f'\, d\eta\right) - \frac{bU_m'}{U_m}\left(f^2 + f'\int f\, d\eta\right) \tag{5}$$

If the jet is self-similar, the velocity and the expansion rate must only be functions of the distance traveled (z), so functions of the form:

$$U_m \propto z^p \qquad b \propto z^q \tag{6}$$

are expected. The exponents p and q are determined by substituting the expressions of Eq. 6 into Eq. 5 and looking only at the variables that vary with z. The result is:

$$z^0 \propto z^{q-1} \tag{7}$$

Since the lefthand side of Eq. 7 is a constant, the righthand side of Eq. 7 must also be a constant. For this to occur, q must equal 1. To find p, we use the momentum integral constraint, which is

$$\frac{d}{dz}\int \rho U^2 2\pi r\, dr = -\pi R\rho\overline{uv} \tag{8}$$

Substituting the variables of Eq. 3 into Eq. 8 and assuming that the Reynolds stress is negligible gives:

$$\frac{d}{dz}\int bU_m^2 f^2\, d\eta = 0 \tag{9}$$

The solution to the integral in Eq. 9 must be a constant. Using the variables defined in Eq. 6 and separating the z dependent variables:

$$bU_m^2 \propto z^{2p} z^q \propto z^0 \tag{10}$$

Since the righthand side of the equation is a constant and q is 1, p must be equal to -0.5. The results for the velocity decay and the jet expansion for the internal annular wall jet thus become:

$$\frac{U_m}{U_s} \propto \frac{1}{\sqrt{z/S}}. \tag{11}$$

$$\frac{b}{S} \propto \frac{z}{S} \tag{12}$$

Here, U_s is the slot velocity, or the source velocity in the jet, S is the width of the slot, and z is the distance the jet has traveled from the origin.

The jet scaling in Eqs. 11 and 12 is consistent with *external* cylindrical wall-jet results for a large cylinder, $R \gg b$ (Starr and Sparrow, 1967; Rajaratnam, 1976). The *internal* annular jet solution has not previously been examined.

Self-similar velocity profile

In order to obtain similarity solutions for the velocity profile, both the zero free stream velocity and the flow-reversal boundary conditions are considered. The derivation for both cases is similar, except that the boundary condition for large η is changed. The free jet boundary condition at large y has the jet slowly approaching a velocity of zero ($U/U_m = 0$ at $\eta = \infty$) as shown in Figure 1a; however, in the case of the flow reversal and recirculation shown in Figure 1b, the velocity quickly goes to zero and then reverses in order to preserve a constant total mass flow across the cylinder. This leads to the boundary condition $U_R/U_m =$ finite and negative at $\eta = R/b$. In both cases, the axisymmetry of the flow requires that $\partial U/\partial y = 0$ at $y = R$.

At the wall of the cylinder, the velocity must equal zero and a boundary layer will develop. This is the *inner* layer of the jet, which is modeled using a boundary-layer profile matched to the jet flow at its outer edge. In a wall jet, the boundary layer grows linearly with distance, so its thickness will scale with z in exactly the same way as the jet half-width b. The boundary- or inner-layer thickness is characterized as δb. The *outer* layer of the jet begins at $y = \delta b$, where $U = U_m$. The outer layer is governed by free jet theory, and it is this layer that will dominate the flow in the bulk of a stirred tank.

The similarity profile for a 2-D jet begins with the equations of motion in their reduced 2-D form:

$$U\frac{\partial U}{\partial z} + V\frac{\partial U}{\partial y} = \frac{1}{\rho}\frac{\partial \tau}{\partial y}. \tag{13}$$

This equation is valid for internal annular wall jets as long as the tank diameter is much greater than the jet width so that the curvature of the wall can be neglected. The similarity solution for the jet profile is derived using the Prandtl approximation for the turbulent shear stress, according to Goertler (1942):

$$\tau = \rho\nu_T\frac{\partial U}{\partial y} \tag{14}$$

Here, ν_T is the kinematic eddy viscosity, and it is assumed that $\rho\nu_T \gg \mu$. Goertler further assumed that the eddy viscosity is proportional to the local maximum velocity and the half-width of the jet:

$$\nu_T \propto U_m b \tag{15}$$

From this, Goertler found that the dimensionless velocity was a function of the distance traveled as well as transverse location in the jet:

$$\frac{U}{U_m} = f'\left(\frac{y}{b}\right) = f'(\eta) \tag{16}$$

Here, y is the distance from the center of the jet, b is the half-width of the jet (a function of the distance the jet has traveled), and $f'(\eta)$ is the similarity function of the velocity. Substituting this information into the equations of motion (Eq. 13), the integrated form becomes:

$$f^2 + f' = A \tag{17}$$

Applying the boundary conditions in Table 1 for a jet in a stagnant fluid, Goertler's (1942) similarity solution is obtained:

$$f' = \frac{U}{U_m} = 1 - \tanh^2(\phi\eta). \tag{18}$$

To force the solution through $U/U_m = 0.5$ at $\eta = 1$, ϕ must be set to 0.88. This solution works very well for free plane jets in a stagnant fluid (Rajaratnam, 1976).

We now consider the similarity solution for a 2-D internal annular jet. Where $b \ll R$, the effect of curvature can be neglected and the equations for the plane jet can be applied. The derivation is similar to the Goertler solution, but the boundary conditions at large η have changed to allow for a negative axisymmetric velocity at the center of the cylinder, as given in Table 2, boundary conditions III and IV. Note

Table 1. Boundary Conditions for a Free Jet in a Stagnant Fluid

(I)	$y = 0$	$\eta = 0$	$U/U_m = f'(0) = 1$
(II)	$y = 0$	$\eta = 0$	$\tau = 0$
(III)	$y = 0$	$\eta = 0$	$V = 0$
(IV)	$y = \infty$	$\eta = \infty$	$f' = 0$
(V)	$y = \infty$	$\eta = \infty$	$\frac{df'}{d\eta} = 0$

Table 2. Boundary Conditions for a Wall Jet in Recirculating Flow

(I)	$y = 0$	$\eta = 0$	$U/U_m = f'(0) = 1$
(II)	$y = 0$	$\eta = 0$	$\tau = 0$
(III)	$y = 0$	$\eta = 0$	$V = 0$
(IV)	$y = R$	$\eta = R/b$	$f' =$ finite value
(V)	$y = R$	$\eta = R/b$	$\dfrac{df'}{d\eta} = 0$

that boundary conditions, I, II, and III ignore the inner boundary layer, assuming that it is thin enough to have a negligible effect on the solution for the outer wall-jet layer. Based on these boundary conditions, the similarity solution becomes:

$$\frac{U}{U_m} = 1 - B\tanh^2(\phi\eta) \tag{19}$$

As $\eta \to \infty$, $\tanh(\eta) \to 1$, so B can *only* be used to capture the recirculating velocity, U_R, at large η.

$$B = 1 - \left(\frac{U_R}{U_m}\right) \tag{20}$$

Since U_R is negative, B is a positive number greater than one. As in Eq. 18 for the free jet, ϕ is used to force the solution through $U/U_m = 0.5$ at $\eta = 1$. In the recirculating jet, ϕ must also compensate for the magnitude of B so it may take on a whole range of values, as shown in Figure 2. Notice that the similarity profiles are virtually identical from the maximum velocity in the jet up to the half-width of the jet. After this point, the recirculation velocity embedded in B dominates the velocity profile. This effect is most easily captured by y_o, the point of flow reversal.

The last issue to be addressed is the displacement of the jet by the inner boundary layer of thickness δb. The measured half-width, b, includes the thickness of the boundary layer, as does y, the distance from the wall. In order to apply

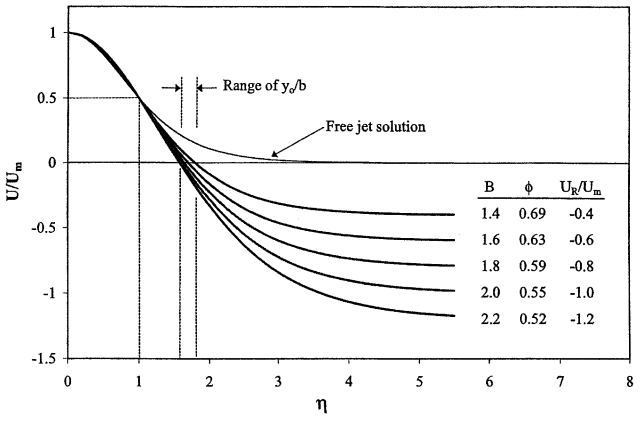

Figure 2. Similarity solutions for the axial velocity profile in the annular wall jet with recirculation.

The constant B increases with the maximum recirculation velocity, U_R.

Eq. 19 in the presence of the boundary layer, it is modified to the following form:

$$\frac{U}{U_m} = 1 - B\tanh^2\left[\Phi(\eta - \delta)\right] \tag{21}$$

where

$$\eta = \frac{y}{b}$$

$$y = y_{\text{jet}} + \delta b$$

$$b = b_{\text{jet}} + \delta b = (1 - \delta)b + \delta b$$

$$\Phi = \phi\frac{b}{b_{\text{jet}}} \tag{22}$$

The solution for the internal annular jet can be summarized with Eqs. 11, 12 and 21. Equation 11 gives the velocity decay, Eq. 12 gives the jet expansion, and Eq. 21 gives the velocity profile. If the boundary-layer thickness is zero, Eq. 21 reduces to Eq. 19, and if U_R is also zero, Eq. 21 further reduces to Eq. 18.

Annular jet in a stirred tank

The radial discharge stream from a Rushton turbine is a swirling radial jet, leaving the tip of the impeller blades at an angle of 45° to the radial direction (Kresta and Wood, 1991). The jet flows rapidly toward the wall of the stirred tank, as indicated by the velocity vector in Figure 3a. As the discharge stream travels toward the tank wall, the angle between the velocity and radial direction shrinks, suggesting an impingement angle of $\beta = 14°$ at the wall for a $D = T/3$ impeller. For a $D = T/2$ impeller, $\beta = 20°$; and for a $T/4$ impeller, $\beta = 10°$. The baffles damp out the small remaining angular component of the flow. The flow divides at the tank wall, flowing axially toward the top and bottom of the tank, as shown in Figures 3b and 3c. The experiments that follow will show that two annular wall jets result: one above the impeller and one below.

For the stirred tank, the momentum source for the wall jets is not flow through an annular slot but a jet core velocity, U_{core}, due to the impeller discharge stream. The core velocity is the global maximum velocity in the wall jet. The slot width, S, is unknown, but if a general annular wall jet exists, S will scale with the tank diameter T. Scaling with T means that the position along the jet will be given in terms of the fraction of the tank diameter traveled, rather than in terms of the number of slot widths downstream of the momentum source. The jet equations become:

$$\frac{U_m}{U_{\text{core}}} \propto \frac{1}{\sqrt{z/T}} \tag{23}$$

$$\frac{b}{T} \propto \frac{z}{T} \tag{24}$$

$$\frac{U}{U_m} = 1 - B\tanh^2\left[\Phi(\eta - \delta)\right] \tag{25}$$

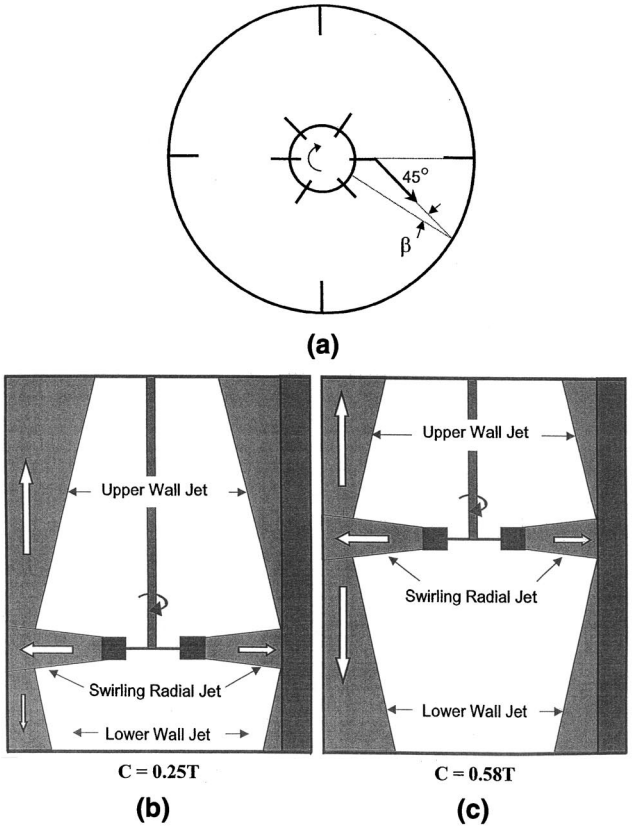

Figure 3. Location of the jets in a stirred tank with a $D = T/3$ Rushton turbine.

(a) The plan view shows the impingement of the swirling radial jet on the wall of the tank; the angle β is the deviation from the radial direction; (b) experimental configuration for measurements in the upper wall jet; (c) experimental configuration for measurements in the lower wall jet.

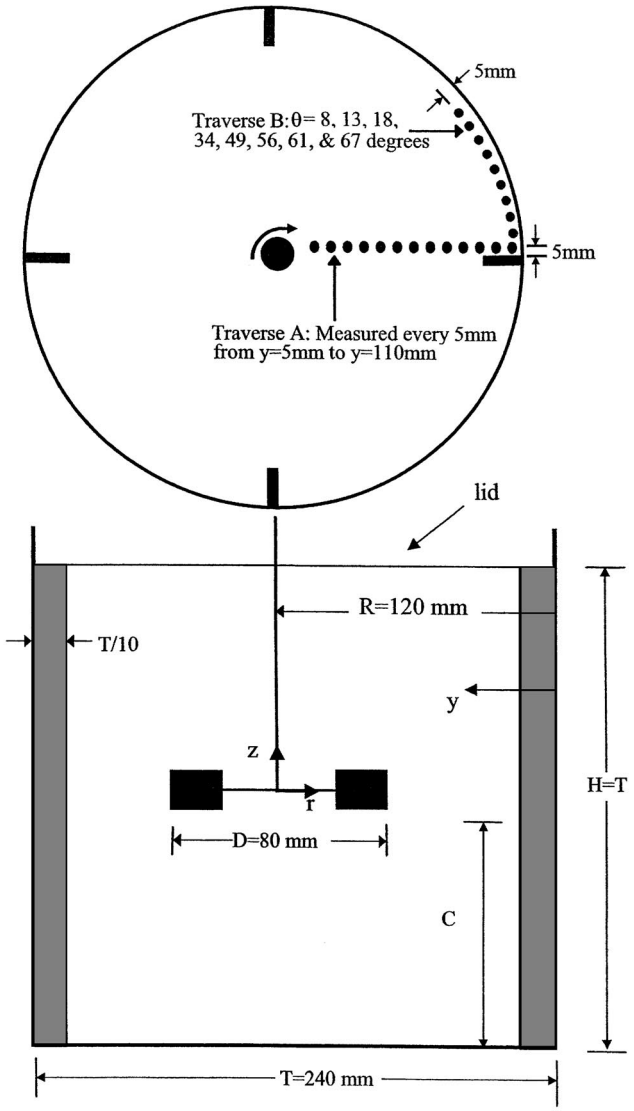

Figure 4. Tank with notation and measurement positions.

The plan view shows the two measurement traverses. The similarity profiles are taken from Traverse A; Traverse B is used to evaluate the axisymmetry of the jet.

Experimental Design

The objective of the experiments is to measure key velocity profiles in the stirred tank in order to test the annular wall-jet hypothesis. Once axisymmetry is established, the experiments focus on the similarity profile of axial velocity, U/U_m vs. y/b, the decay of the local maximum velocity, U_m, and the expansion of the jet as characterized by the half-width, b. Two cases were examined, a low clearance case ($C = 0.25T$, Figure 3b), where the focus was on the upper jet, and a high clearance case ($C = 0.58T$, Figure 3c), where the focus was on the lower jet. This allows generalization of the annular jet beyond the standard geometry where $C = T/2$. More importantly, it increases the length of an individual annular jet, allowing a better test of the velocity decay. The tank and the measurement traverses are shown in Figure 4. Traverse A is the cross section of the jet, and Traverse B is used to test for axisymmetry. Axial locations are defined relative to the impeller disk plane at the center of the blades (z in Figure 4). For the low clearance case, the space above the impeller extends from $z/T = 0$ to $z/T = +0.75$. Measurement traverses were located at $z/T = 0.10$, 0.21, 0.31, 0.42, and 0.52. For the high clearance case, the space below the impeller extends from $z/T = 0$ to $z/T = -0.58$ and traverses were located at $z/T = -0.08$, -0.19, -0.29, and -0.40.

Mean and fluctuating axial velocities were measured using the laser Doppler velocimeter (LDV), as specified in Table 3. The equipment settings and experimental parameters are described in detail in Bittorf and Kresta (2000) and Zhou and Kresta (1996). The reader should take special note of the data-collection conditions. In regions near the top of the tank, very long measuring times and a large sample size are required. The velocities in this part of the tank can be quite low. As a result the number of seeding particles crossing the measuring volume drops significantly, leading to data rates as low as 200 Hz and long sampling times for each velocity record. A long record length is also necessary to ensure that

Table 3. Summary of Experimental Conditions

LDV	300-mW Argon laser, $\lambda = 514.5$ nm Beam separation = 0.0340 m Focal length = 500 mm Fringe spacing = 7.6 μm Bragg cell frequency shift = 40 MHz Velocity variability = $\pm 5\%$
Positioning	Horizontal traverses Computerized: accuracy = ± 0.25 mm Vertical traverse Manual: accuracy = ± 1.0 mm Off-bottom clearance traverse Manual: accuracy = ± 0.5 mm
Data Collection	Working fluid: tap water Seeding: 1 μm particulate in tap water Data rate = 200 Hz to 2 kHz Sample size = 10,000 to 125,000 points
Geometry	Rushton Turbine, standard geometry blade thickness = 0.9 mm $D = T/3$ Cylindrical tank $T = 240$ mm 4 baffles, baffle width = $T/10$ $C = 0.25\ T$ and $0.58\ T$ Fully turbulent flow $Re = 5.33 \times 10^4$ $N = 500$ rpm

enough large-scale velocity fluctuations are captured to provide a meaningful average velocity (Roussinova et al., 2000). All velocity records are one minute long: sample sizes vary from 10,000 to 125,000 points.

Results

As was stated in the Introduction, proof of the annular jet hypothesis will require three conditions: axisymmetry of the flow at the wall, self-similar velocity profiles that scale with the characteristic velocity and length scales U_m and b, and decay of those scales as $U_m \propto 1/z^{0.5}$ and $b \propto z$, where z is the distance along the jet. If the hypothesis is satisfied, Eqs. 23–25 will complete the similarity solution. Experimental input to these equations is limited to three parameters: the value of B and the proportionality constants required for Eqs. 23 and 24. As an initial probe of the turbulence in the wall jet, profiles of u/U_m are examined for similarity. This last test is more difficult to achieve than similarity in the mean flow, since the fluctuating velocities will not become self-similar until after similarity in the mean velocity is well established.

Axisymmetry

First, the assumption of a 2-D flow is examined in a traverse over the θ-direction progressing away from the baffle (Figure 4a, Traverse B). The dimensionless axial velocity measurements are shown in Figure 5. The velocities are within $\pm 10\%$ of the local maximum velocity at all angular positions, with apparently random variations. Based on these results, the model of an axisymmetric system was accepted. The implication of this is that the baffles serve a somewhat different purpose in a radial flow (from a Rushton turbine) than in a axial flow (from a fluid foil, or low clearance pitched-blade impeller). For an axial impeller, the baffles concentrate the upward flow in a 3-D jet (Bittorf and Kresta, 2001), but for a radial impeller the baffles simply damp out the remaining tangential motion in the impeller discharge stream.

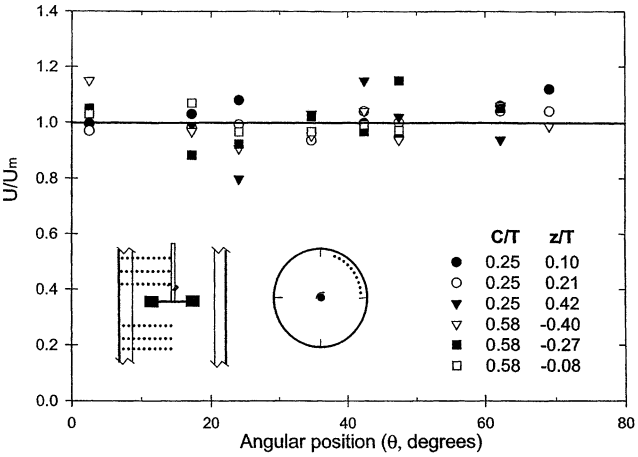

Figure 5. Axial velocity profile along the tank wall showing no systematic deviations from axisymmetry in the annular jet.

Jet decay and expansion

The similarity scaling in Eqs. 23 and 24 specifies a velocity decay proportional to $1/z^{0.5}$ and a linear expansion of b with z in the annular wall jet. The distances in these scaling equations are referred back to a virtual origin, z_o, the point at which the width of the jet shrinks to zero and the momentum is injected from a line source of zero width. The virtual origin is found by extrapolating the half-width data back to the point where $b = 0$. For the upper wall jet, $z_o/T = -0.33$; for the lower wall jet, $z_o/T = +0.36$. Although the difference in these values may not seem large, results for the 3-D jet show that z_o is a function of geometry. Both values are retained, as they will make a significant difference in the scaling of the jet decay and expansion.

The velocity decay provides a test of the difference between the 3-D jet observed for axial impellers and the annular jet hypothesized for radial impellers. The experimental data for both the upper and lower jet are combined in Figure 6, where the core velocities and virtual origins for both jets are reported. The core velocity, U_{core}, is located roughly $0.2T$ above/below the impeller plane, and is approximately 25% of the impeller tip speed. The velocity decay agrees very well with Eq. 23, giving:

$$\frac{U_m}{U_{\text{core}}} = \frac{0.74}{\sqrt{\left(\left|\frac{z}{T}\right| + \left|\frac{z_o}{T}\right|\right)}} \tag{26}$$

The internal annular wall jet can be described as expanding from a ring source of mass and momentum. Since a jet originating from a theoretical point source always spreads faster than a jet originating from a continuous or line source (Rajaratnam, 1976), the annular jet is expected to expand at a much slower rate than the 3-D wall jet due to the axial

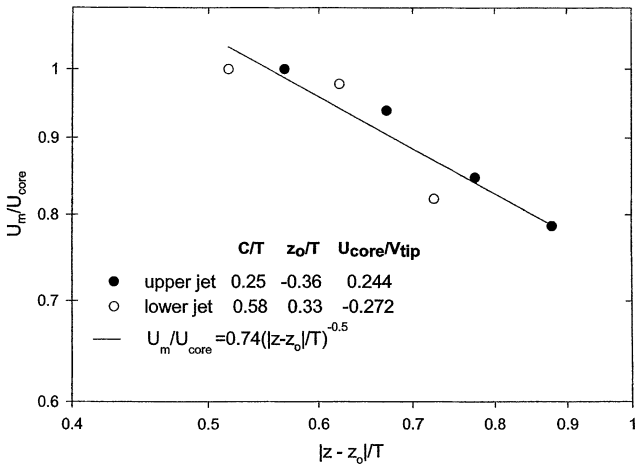

Figure 6. Decay of maximum jet velocity U_m, for the annular wall jet with recirculation produced by Ruston turbine at two off-bottom clearances.

The decay of velocity closely matches the similarity scaling for both the upper and the lower wall jet.

impeller. The data are in agreement with this result. The virtual origin of the annular jet is $0.36T$ below the center line of the impeller for the upper jet and $0.33T$ above the center line of the impeller for the lower jet. The angle of expansion is roughly 10° for both jets. This completes the equations for b, based on Eq. 24:

$$\frac{b}{T} = 0.19\left(\left|\frac{z}{T}\right| + \left|\frac{z_o}{T}\right|\right) \qquad \frac{z_o}{T} = -0.36 \text{ or } +0.33 \quad (27)$$

This can be contrasted with the results for the 3-D wall jet driven by axial impellers (Bittorf and Kresta, 2001), where the jet originates from a point source from $0.07T$ to $0.12T$ below the bottom of the tank, and spreads at an angle of 20°, exactly twice as fast as the spread of the annular jet:

$$\frac{b}{T} = 0.38\left(\left|\frac{z}{T}\right| + \left|\frac{z_o}{T}\right|\right) \qquad -0.07 < \frac{z_o}{T} < -0.12 \quad (28)$$

The wall jet driven by the Rushton turbine has a slower decay of axial velocity than the 3-D wall jet driven by axial impellers, which decays as $1/z$ (Bittorf and Kresta, 2001). In addition, the Rushton turbine is often placed at $C = T/2$, so the annular jet typically traverses only $0.5T$, rather than the full height of the tank, as is the case for down pumping axial impellers. This supports the general observation that the Rushton turbine drives a much stronger circulation throughout the tank than axial impellers, and goes beyond this to allow calculation of the circulation at various heights in the vessel. This suggests an explanation for many experimental findings where, in spite of careful matching of the turbulence (or power dissipation per mass), the results for axial and radial impellers follow somewhat different trends, while the results for all axial impellers collapse extremely well. The annular wall jet extends all the way around the tank wall and penetrates further into the bulk of the tank at a higher velocity than the 3-D wall jet.

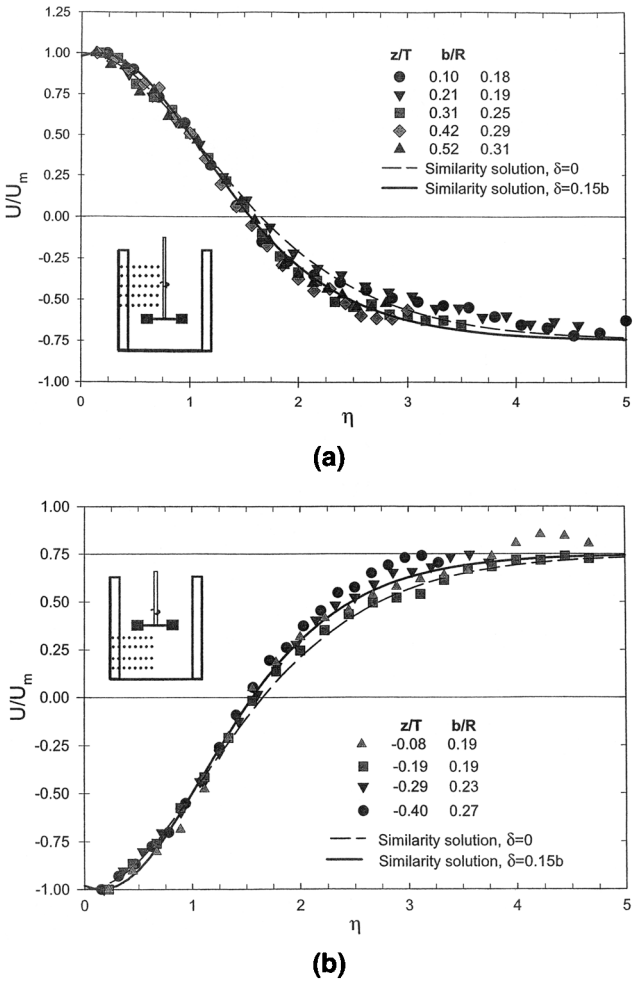

Figure 7. Self-similar profiles of axial velocity in the annular wall jet for $Re = 5 \times 10^4$.

The data suggest $B = 1.75$ with $\delta = 0.15$b in Eq. 21; this requires $\Phi = 0.702$. (a) Upper wall jet: $C = 0.25T$; (b) lower wall jet: $C = 0.58T$.

Similarity profiles

Figures 7a and 7b show the similarity scaling of axial velocity profiles in the upper and lower wall jets, respectively. The collapse of the profiles is excellent up to $\eta = 2.0$, and good throughout. In identifying the best form of Eq. 25 for a similarity solution, there are three parameters to select: B, Φ, and δ. Figures 7a and 7b suggest a single value of B due to the recirculation velocity, U_R. To examine this more closely, the profiles are rescaled with y/T in Figures 8a and 8b. The reader will observe two things from Figure 8: first, all of the profiles asymptote to a single value of $U_R = -0.75U_m$; second, the jet scaling (y/b) provides a much better collapse of the data than the external scaling (y/T) over most of the profile. The most important conclusion to draw from Figure 8 is that there is a single characteristic velocity scale, U_m, in the annular jet, and it is this velocity scale that drives the recirculating flow.

Given a single value of B, Figure 2 and Eq. 19 suggest a unique value of y_o. Any variation in y_o must then be due to the presence of a boundary layer of thickness δb in Eq. 25.

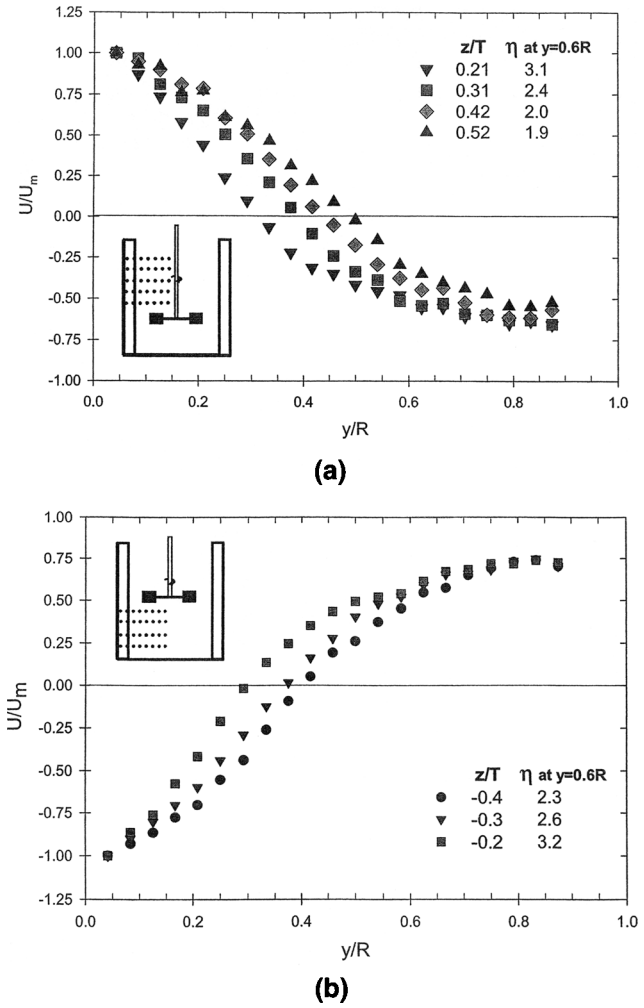

Figure 8. Scaling of the axial velocity profiles from Figure 7, with an alternate length scale, *R*.

The collapse of the data is good only in the constant velocity recirculation zone starting at $y = 0.75R$. (a) Upper wall jet: $C = 0.25T$; (b) lower wall jet: $C = 0.58T$.

Returning to Figures 7a and 7b, two similarity solutions are shown: one for $\delta = 0$ and one for $\delta = 0.15b$, a typical value for wall jets. The boundary-layer solution is clearly the better of the two at the critical y_o position. The third parameter, Φ, is now fully specified by the condition $U/U_m = 0.5$ at $\eta = 1.0$, giving $\Phi = 0.702$. With the value of B as the single experimentally determined parameter, Eq. 25 becomes:

$$\frac{U}{U_m} = 1 - 1.75 \tanh^2 \left[0.702(\eta - 0.15)\right] \qquad (29)$$

These results clearly show that the flow in the bulk of the tank is driven by the annular wall jets, and that this entire section of the flow can be scaled with U_m and b. Equations 25 and 27 for the decay of U_m and the expansion of b are expected to have general applicability for radial flow in a tank.

If the similarity profile in Eq. 29 is combined with the inner boundary layer and mass continuity is applied over a cross section of the tank, the jet half-width is constrained to a single value: $b/R = 0.17$. A similar constraint applied to a momentum balance between the upward and downward flows gives $b/R = 0.16$. Details of the calculations are given in the Appendix. Experimental values given in Figure 7 range from $0.18 < b/R < 0.31$. This suggests that there is a small 3-D element to the flow that is not captured by the experimental data.

The remaining undefined variable is U_{core}, which scales directly with the rotational speed of the impeller, N. The reader can reasonably expect that U_{core} will show some dependence on the ratio of impeller diameter to tank diameter and on the geometry of the radial impeller selected. There is a small difference between the core velocities for the two jets, emphasizing the importance of geometry to the initial conditions in the jet. For $C = 0.25T$, the jet flows upwards and $U_{\text{core}} = 0.244V_{\text{tip}}$. For $C = 0.58T$, the flow is downward and $U_{\text{core}} = -0.272V_{\text{tip}}$. These velocities are similar in magnitude to the core velocities reported for axial impellers, which range from $0.210V_{\text{tip}}$ to $0.326V_{\text{tip}}$ (Bittorf and Kresta, 2001).

Turbulent intensities

The final property examined for the internal annular wall jet was the axial turbulence intensity, shown in Figure 9. The results from this figure are similar to the results obtained from the 3-D wall jet in a stirred tank (Bittorf and Kresta, 2001). As was the case for the axial impeller, similarity in the fluctuating velocities does not occur until the decay of the mean velocity is well established. The mean velocities exhibit similarity at $z/T = 0.1$, while the fluctuating velocity profiles continue to develop up to $z/T = 0.41$. Other authors have also reported that a longer distance is needed to establish similarity of the fluctuating velocities (Padmanabham and Gowda, 1991; Swamy and Bandyopadhyay, 1975; and Newman et al., 1972). Because of the relatively short distances in a stirred tank, much of the wall jet will contain a turbulent component that is still developing.

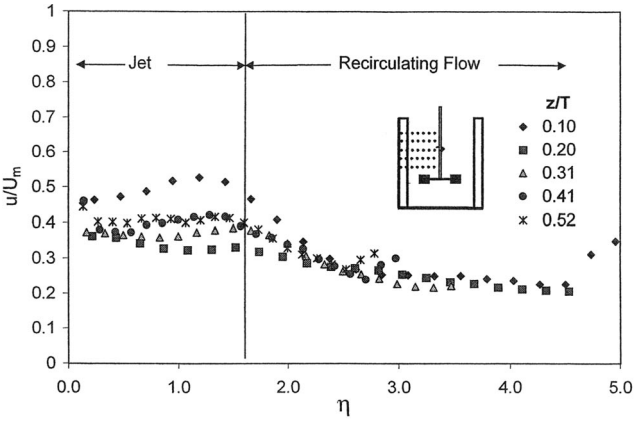

Figure 9. Turbulence intensity in the internal annular wall jet for $D = 0.33T$, $C = 0.25T$, $N = 500$ rpm, and $Re = 5 \times 10^4$.

Above $z/T = 0.41$ the turbulence intensity profiles are self-similar, and for $\eta > 3.0$ in the recirculating flow the *scaled* turbulence intensity is constant at $0.4U_m$.

The reader will note that the mean velocity gradient in the recirculating flow is essentially zero for $y > 0.6R$, so the turbulence intensity will be small. This is borne out by the results in Figure 9, which show that for $\eta > 2.5$, the intensity of turbulence is much smaller than that close to the wall, dropping to less than one-third of the intensity measured at the impeller (Zhou and Kresta, 1996). Unfortunately, this is a region of significant practical importance when surface feed is necessary and rapid mixing is desirable. While these data are limited, they establish a level of turbulence at the wall of the tank for the Rushton turbine and in the recirculating flow.

Implications

The experimental results strongly support the hypothesis that an annular wall jet exists at the wall of the tank, and that the wall jet drives the recirculating flow in the center of the tank. The axial velocity profiles from $z = \pm 0.1T$ above (below) the plane of the impeller to $0.2T$ from the top (bottom) of the tank are defined by a single, self-similar velocity profile (Eq. 29), which scales with the peak velocity in the wall jet, U_m, and the half-width of the jet, b. The decay of the local maximum velocity, U_m, is described by Eq. 26, and the expansion of jet half-width, b, by Eq. 27. The recirculation velocity, U_R, is not independent but scales well with U_m. As long as the flow is fully turbulent and strict geometric similarity is obeyed, Reynolds laws of kinematic similarity will hold and all velocities will scale with N, the rotational speed of the impeller. The only variables in the model that depend on the specifics of the tank geometry are U_{core}, the global maximum velocity in the jet, and z_o, the virtual origin of the jet. If the impeller geometry, impeller diameter, or off-bottom clearance of the impeller are changed, a single velocity traverse at $z = 0.2T$ (the expected location of U_{core}), would fix U_{core} and z_0. Validation of the similarity profile from the same data provides assurance of the accuracy of U_R and y_o. Everything needed to predict the axial velocity over the annular jet region would then be in place. The implications of this description of the flow for solids distribution and turbulence scaling in the bulk of the tank, and development of quantitatively accurate CFD models, are of significant practical importance.

Prediction of solids distribution throughout a stirred tank is a problem quite distinct from that of complete suspension of solids off the bottom of the tank. At high solids concentrations, many fully suspended solids will develop an interface below which the solids concentration is fairly uniform and above which there are very few solid particles. Prediction of the location of this interface is required for applications such as slurry catalyst reactors (Bujalski et al., 1999). Bittorf (2000) has shown that the position of the interface can be determined using the decay of U_m in the wall jet. The interface forms at the point where U_m is equal to a fraction of the impeller tip speed at just suspended conditions, suggesting a balance between the upward velocity in the wall jet and the settling characteristics of the particles.

The annular wall-jet model suggests an appropriate integral length scale to use for turbulent scaling in the bulk of the tank. The half-width of the jet, b, is either equal to or proportional to the size of any large-scale vortices in the jet. The jet half-width, b, also scales both the point of flow reversal, y_o, which is the thickness of the gross circulation loop in the tank, and the thickness of the boundary layer at the wall, δ. Regardless of whether gross circulation, flow in the wall jet, or flow in the boundary layer dominates, the half-width of the annular wall jet (adjusted by at most a proportionality constant) defines the scaling of the flow in the jet. In the recirculating flow, another integral length scale may dominate, bearing in mind the results in Figure 8. From $0.75R < y < R$, the velocity profiles collapse better when scaled with R than when scaled with b. The radius of the constant velocity recirculation flow is approximately $0.25R$, suggesting a second independent length scale.

Another application of the annular jet model is its use in the validation and development of CFD modeling. The application of CFD to flow in stirred tanks is a well-developed field, with several modeling schemes specifically designed for this application. In general, CFD predictions of trends are very good, but quantitative agreement, particularly in the bulk of the tank, is not adequate. Assessment of models for the flow in the bulk of the tank has been limited by a lack of understanding of the driving mechanisms in this part of the tank. If CFD is to be used in a predictive sense, it must accurately predict three key aspects of the flow. In the developing wall jet, U_{core} and z_o define the momentum source for a specific tank geometry. In the similarity profile, the boundary-layer thickness, δ, the point of flow reversal, y_o, and the recirculating velocity, U_R, must scale correctly with the half-width, b, and the maximum velocity, U_m. As the jet travels along the wall, the decay of U_m and the expansion of b complete the definition of the mean velocity field. Predicting the decay of the wall jet would be a stringent test of a CFD simulation, as the expansion and decay of the jet are dominated by the performance of the turbulence model.

Conclusions

In this article, equations were developed for an internal annular wall jet with and without recirculating flow. The resulting model was compared to the flow at the wall of a stirred tank: specifically, for a Ruston turbine impeller at two different off-bottom clearances. The experimental results strongly support the annular wall-jet model (Eqs. 26, 27, and 29) from $z = \pm 0.1T$ above (below) the impeller plane to approximately $0.2T$ from the top (bottom) surface. The conclusions to be derived from the model and experimental results are as follows:

- A pair of axisymmetric annular wall jets is formed at the tank wall when the flow is driven by a Rushton turbine radial impeller. One jet flows upward, the other flows downward.
- Both annular wall jets scale with a single velocity, U_m, throughout the jet and the recirculating flow. The recirculating velocity, U_R, is a constant fraction of U_m.
- The half-width of the jet, b, defines the scaling of the jet through the boundary layer and beyond the point of flow reversal, y_o. The size of the constant velocity recirculation zone appears to scale with $0.25R$. This provides a good starting point for identifying the largest scales of turbulence in the bulk of the tank.
- The upward (downward) flowing annular wall jet is axisymmetric and the velocity decay is proportional to the

square root of the distance traveled. This is contrasted with the flow driven by axial impellers, where four distinct 3-D wall jets form at the baffles and the velocity decays with $1/z$. Given the same core velocity, the annular wall jets driven by the Rushton turbine will generate more circulation in the bulk of the tank than the 3-D wall jets driven by axial impellers.

These results have implications for the prediction of solids distribution, for scaling the flow field, and for interpreting CFD results throughout the bulk of the tank.

Notation

A = constant
b = jet half-width, distance from the wall where $U = U_m/2$ (L)
b_{jet} = distance from U_m to $U_m/2$ (L)
B = similarity constant $B = 1-(U_R/U_m)$
C = clearance (L)
c_f = skin friction coefficient
D = impeller diameter (L)
f' = similarity function for dimensionless velocity
f = integral of f'
g = dimensionless Reynolds stress
M = momentum flux ($M\,L\,t^{-2}$)
N = impeller speed (rotations per second, t^{-1})
N_{js} = impeller speed at just suspended conditions (rotations per second, t^{-1})
p = exponent in similarity solution
Q = volumetric flow rate (L^3t^{-1})
Q_{BL} = volumetric flow rate in the boundary layer (L^3t^{-1})
q = exponent in similarity solution
r = radial coordinate (L)
Re = impeller Reynolds number (ND^2/ν)
Re_s = slot Reynolds number (SU_s/ν)
R = cylinder and tank radius (L)
S = annular slot width, see Figure 1 (L)
T = tank diameter (L)
U = streamwise (z) velocity ($L\,t^{-1}$)
U_R = maximum (countercurrent) velocity in the recirculating flow ($L\,t^{-1}$)
U_{core} = jet-core velocity; global maximum velocity in the jet ($L\,t^{-1}$)
U_s = annular slot or source velocity; see Figure 1 ($L\,t^{-1}$)
u = fluctuating component of axial velocity ($L\,t^{-1}$)
U_m = maximum jet velocity at a fixed z ($L\,t^{-1}$)
U_{mCH} = maximum jet velocity at the solids cloud height ($L\,t^{-1}$)
u^+ = dimensionless velocity in the boundary layer
u^* = shear velocity ($L\,t^{-1}$)
v = fluctuating component of radial velocity ($L\,t^{-1}$)
V = cross stream (y or r) velocity component ($L\,t^{-1}$)
V_{tip} = impeller tip speed (πND) ($L\,t^{-1}$)
W = cross stream (x or θ) velocity component ($L\,t^{-1}$)
x, y, z = Cartesian coordinates (L)
y^+ = dimensionless distance in the boundary layer
y = distance from tank wall (L)
y_{jet} = distance from U_m position in the jet (L)
y_o = y position at which velocity is zero (L)
z = axial coordinate (L)
z_o = virtual origin of the jet (L)

Greek letters

α = constant from Glauert (1956)
β = angle of deviation from the radial direction (deg)
δ = boundary layer thickness (L)
ϕ = similarity constant in the absence of a boundary layer
Φ = similarity constant associated with finite boundary-layer thickness
η = dimensionless distance (y/b)
λ = wavelength of laser light (L)
μ = viscosity ($M\,L^{-1}\,t^{-1}$)
ν = kinematic viscosity ($L^2\,t^{-1}$)
ν_T = kinematic eddy viscosity ($L^2\,t^{-1}$)
θ = tangential coordinate (deg)
ρ = density ($M\,L^{-3}$)
τ = turbulent stress ($M\,L^{-1}\,t^{-2}$)
τ_w = shear stress at the wall ($M\,L^{-1}\,t^{-2}$)

Literature Cited

Abrahamsson, H., B. Johansson, and L. Lofdahl, "A Turbulent Plane Two-Dimensional Wall-Jet in a Quiescent Surrounding," *Eur. J. Mech., B/Fluids*, **13**, 533 (1994).

Bakke, P., "An Experimental Investigation of Wall Jet," *J. Fluid Mech.*, **2**, 467 (1957).

Bittorf, K. J., *The Application of Wall Jets in Stirred Tanks*, PhD Thesis, Univ. of Alberta, Edmonton, Alta., Canada (2000).

Bittorf, K. J., and S. M. Kresta, "Three Dimensional Wall Jets: Axial Flow in a Stirred Tank," *AIChE J.*, **47**, 1277 (2001).

Bittorf, K. J., and S. M. Kresta, "Active Volume of Mean Circulation for Stirred Tanks Agitated with Axial Impellers," *Chem. Eng. Sci.*, **55**, 1325 (2000).

Bujalski, W., K. Takenka, S. Paolini, M. Jahoda, A. Paglianti, K. Takahashi, A. W. Nienow, and A. W. Etchells, "Suspensions and Liquid Homogenisation in High Solids Concentration Stirred Chemical Reactors," *Trans. Inst. Chem. Eng.*, **77**, 241 (1999).

Chao, J. L., and V. A. Sandborn, "Evaluation of the Momentum Equation for a Turbulent Wall Jet," *J. Fluid Mech.*, **26**, 818 (1966).

Eriksson, J. G., R. I. Karlsson, and J. Persson, "An Experimental Study of a Two-Dimensional Plane Turbulent Wall Jet," *Exp. Fluids*, **25**, 50 (1998).

Gerodimos, G., and R. M. C. So, "Near-Wall Modeling of Plane Turbulent Wall Jets," *J. Fluids Eng.*, **119**, 304 (1997).

Glauert, M. B., "The Wall Jet," *J. Fluid Mech.*, **1**, 625 (1956).

Goertler, V. H., "Berechnung von Aufgaben der frein Turbulenz auf Grund eines neuen Naherungsansatzes," *Z. Angew. Math. Mech.*, **22**, 244 (1942).

Kolar, V., P. Filip, and A. G. Curev, "Similarity Prediction of Wall Jets on Bodies of Revolution," *Acta Mech.*, **76**, 253 (1989).

Kresta, S. M., and P. E. Wood, "Prediction of the Three Dimensional Turbulent Flow in Stirred Tanks," *AIChE J.*, **37**, 448 (1991).

Launder, B. E., and W. Rodi, "The Turbulent Wall Jet," *Prog. Aerosp. Sci.*, **19**, 81 (1981).

Launder, B. E., and W. Rodi, "The Turbulent Wall Jet-Measurements and Modelings," *Ann. Rev. Fluid Mech.*, **15**, 429 (1983).

Newman, B. G., R. P. Patel, S. B. Savage, and H. K. Tjio, "Three-Dimensional Wall Jet Originating from a Circular Orifice," *Aerosp. Q.*, **23**, 188 (1972).

Padmanabham, G., and B. H. Gowda, "Mean and Turbulence Characteristics as a Class of Three-Dimensional Wall Jets—Part 1: Mean Flow Characteristics," *J. Fluids Eng.*, **113**, 620 (1991).

Rajaratnam, N., and B. S. Pani, "Three-Dimensional Turbulent Wall Jets," *Tech. Rep.*, Dept. of Civil Engineering, University of Alberta, Edmonton, Alta., Canada (1970).

Rajaratnam, N., and B. S. Pani, "Three-Dimensional Wall Jets," *Proc. ASCE J. Hydraulics Division*, **100**, 69 (1974).

Rajaratnam, N., *Turbulent Jets*, Elsevier, New York (1976).

Rodman, L. C., N. J. Wood, and L. Roberts, "Experimental Investigation of Straight and Curved Annular Wall Jets," *AIAA J.*, **27**, 1059 (1989).

Roussinova, V., B. Grgic, and S. M. Kresta, "Study of Macro-Instabilities in Stirred Tanks Using a Velocity Decomposition Technique," *Chem. Eng. Res. Des.*, **78**, 1040 (2000).

Schwarz, W. H., and W. P. Cosart, "The Two-Dimensional Wall-Jet," *J. Fluid Mech.*, **10**, 481 (1960).

Sharma, R. N., "Experimental Investigation of Conical Wall Jets," *AIAA J.*, **19**, 28 (1981).

Starr, J. B., and E. M. Sparrow, "Experiments on a Turbulent Cylindrical Wall Jet," *J. Fluid Mech.*, **29**, 495 (1967).

Swamy, N. V., and P. Bandyopadhyay, "Mean and Turbulence Characteristics of Three-Dimensional Wall Jets," *J. Fluid Mech.*, **71**, 541 (1975).

Venas, B., H. Abrahamsson, and P. A. Krogstad, "Pulsed Hot-Wire Measurements in Two- and Three-Dimensional Wall Jets," *Exp. Fluids*, **27**, 210 (1999).

Wilson, B. J., and R. J. Goldstein, "Turbulent Wall Jets with Cylindrical Streamwise Surface Curvature," *J. Fluids Eng.*, **98**, 550 (1976).

Zhou, G., and S. M. Kresta, "Distribution of Energy Between Convective and Turbulent Flow for Three Frequently Used Impellers," *Trans. Inst. Chem. Eng.*, **74**, 379 (1996).

Appendix: Conservation of Mass and Momentum

The 2-D annular jet model can be tested for conservation of mass and momentum by integration over the cross section of the tank at a fixed axial location.
Mass conservation requires:

$$Q = 2\pi \int_0^R U(y - R)\, dy = 0 \tag{A1}$$

Integrating gives

$$Q = Q_{BL} + 2\pi U_m B(R - \delta b)^2 \left[\frac{1}{2} - \frac{1}{2B} + \frac{b}{\Phi(R - \delta b)} + \left(\frac{b}{\Phi(R - \delta b)} \right)^2 \ln \left[\frac{2}{\exp\left(\frac{2\Phi(R - \delta b)}{b} + 1 \right)} \right] \right] \tag{A2}$$

where Q_{BL} is the volumetric flow upward in the boundary layer.

The boundary layer is described by the log law of the wall (Gerodimos and So, 1997):

$$u^+ = y^+ \qquad 0 < y^+ < 10 \tag{A3}$$

$$u^+ = 2.44 \ln y^+ + 5.0 \qquad y^+ = 10 \text{ to } y = \delta \text{ (or } y^+ = u^* \delta / \nu) \tag{A4}$$

Here y^+ is the dimensionless distance and u^+ is the dimensionless velocity:

$$y^+ = \frac{u^* y}{\nu} \qquad u^+ = \frac{u}{u^*} \qquad u^* = \sqrt{\frac{\tau_w}{\rho}} \tag{A5}$$

The shear stress τ_w can be estimated from (Abrahamsson et al., 1994):

$$\tau_w = c_f \frac{1}{2} \rho U_s^2 = 0.0157 Re_s^{-0.182} \rho U_s^2 \tag{A6}$$

This correlation matches data from Eriksson et al. (1998) for a plane wall jet. From Eqs. A3–A6 the volumetric flow rate in the boundary layer can be calculated:

$$Q_{BL} = 2\pi u^* \left(\int_0^{y^+ = 10} y^+ dy + \int_{y^+ = 10}^{\delta b} (2.44 \ln y^+ + 0.5)\, dy \right) \tag{A7}$$

The limits of integration are based on the values calculated from Eqs. A5 and A6. Combining Eqs. A7 and A2 completes the mass balance for a single profile.

A momentum balance can be applied to find the point at which the momentum of the recirculating flow equals the momentum in the jet. If the jet grows beyond this point, the flow is expected to change from jet dominated to recirculation dominated, and the assumption that the diameter of the tank is much greater than the half-width of the jet may be violated. Equating the upward and downward momentum fluxes gives:

$$M = 2\pi\rho \int_0^{y_o} U^2 (y - R)\, dy = 2\pi\rho \int_{y_o}^R U^2 (y - R)\, dy \tag{A8}$$

Both the mass balance and the momentum balance contain a number of unknowns that depend on the geometry of interest. For specified values of B and δ, Φ is fixed: the value of b/R, which satisfies a mass balance or a momentum balance can be calculated from Eqs. A2 and A8, respectively.

Manuscript received Aug. 2, 2000, and revision received May 21, 2001.